

Mesoscopic non-Hermitian skin effect

Alexander Poddubny,^{1,*} Janet Zhong,^{2,†} and Shanhui Fan²

¹*Department of Physics of Complex Systems, Weizmann Institute of Science, Rehovot 7610001, Israel*

²*Department of Applied Physics, Stanford University, Stanford, California 94305, USA*

We discuss a generalization of the non-Hermitian skin effect to finite-size photonic structures with neither gain nor loss in the bulk and purely real energy spectrum under periodic boundary conditions (PBC). We show that such systems can still have significant portions of eigenmodes concentrated at the edges and that this edge concentration can be linked to the non-trivial point-gap topology of the size-dependent regularized PBC spectrum, accounting for the radiative losses. As an example, we consider the chiral waveguide quantum electrodynamics platform with an array of atoms coupled to the waveguide. The proposed mesoscopic analogue of the non-Hermitian skin effect could be potentially applied to other seemingly lossless photonic structures, such as chiral resonant all-dielectric metamaterials.

Introduction. Non-Hermitian skin effect (NHSE) is manifested by the concentration of the eigenmodes at the edge of a finite structure under open boundary conditions (OBC), that is related to the nontrivial point-gap topology under periodic BC [1–7]. Particular realizations of NHSE can be very different, such as tight-binding lattices, photonic crystals [8, 9], continuous media [10], and even lattices in synthetic dimensions [11]. In all these cases, the energy spectrum drastically changes under the open boundary conditions (OBC), contrary to the usual Hermitian systems. A paradigmatic example is the Hatano-Nelson model of one-dimensional lattice with different left- and right-tunneling coupling constants $t_1 \neq t_2$ [12], see Fig. 1(a). Its PBC spectrum has a loop in the complex plane with a non-zero winding number, that under OBC collapses into a line corresponding to edge-concentrated eigenmodes.

Here we apply this NHSE perspective to the edge eigenmode concentration in a very different photonic system, that has purely real PBC spectrum and neither loss nor gain in the bulk, see Fig. 1(b,d). When being put under open boundary conditions, a finite structure still acquires radiative losses due to the photon escape into the far field, so the OBC spectrum becomes complex. These OBC eigenmodes can also concentrate at one edge when the structure is chiral. We aim to link this concentration to the non-trivial point-gap topology of dispersion law $\omega(K)$ for complex wave vectors K . To this end, we propose a regularization of the $\omega(K)$ dependence for a finite structure. The real-valued PBC spectrum is dramatically modified by this regularization. It becomes complex and encircles the OBC spectrum, see horseshoe contours in Fig. 1(d), just like in the usual NHSE case of Fig. 1(c). In stark contrast to the usual scenario, the regularized PBC depends on the system size, so the considered NHSE has a mesoscopic nature.

We consider a particular example of mesoscopic NHSE for the chiral waveguide quantum electrodynamics (QED) setup, that is, for an array of natural or artificial atoms, chirally coupled to the waveguide [13, 14]. Such arrays are now studied both experimentally [15–17] and

theoretically. While they are known to have eigenmodes concentrated at the edges [18–23], we believe that the size-dependent connection to the NHSE is not yet fully understood. In particular, while Ref. [19], with one of us as a coauthor, analyzed the eigenmodes in great detail, this work has not mentioned any topological spectral features. Refs. [22, 23] considered a very similar setup for magnons that, however, had an inherent nonzero non-radiative loss. Refs. [20, 21] did discuss NHSE in substantially different chiral atomic systems, where the main loss mechanism was due to the emission into the free space [20], i.e. perpendicular to the waveguide or perpendicular to the plane of the atomic mirror [21], rather than at the edges. Thus, already the non-regularized PBC spectrum in Refs. [20–23] has been complex corresponding to the usual NHSE case of Fig. 1(a,c) rather than to the proposed mesoscopic NHSE.

Model. We consider single-excited eigenstates in

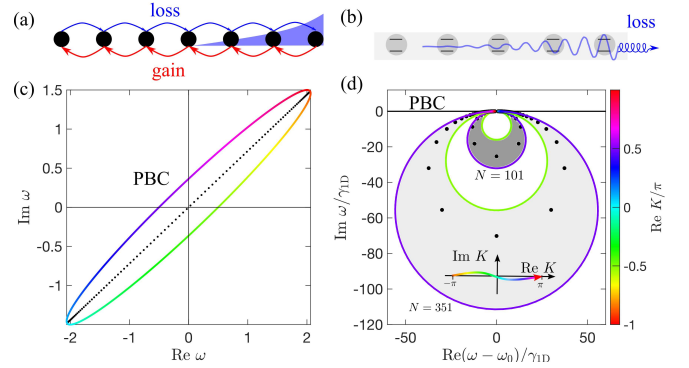


FIG. 1. (a,b) Schematics of (a) Hatano-Nelson model with spatially distributed gain and loss and (b) chiral waveguide-QED model with radiative loss on the edges. (c,d) spectra under periodic boundary conditions (PBC, colored lines) and open boundary conditions (OBC, black dots) in these models. Hatano-Nelson model corresponded to $t_1 = 1 + 0.5i$, $t_2 = 1 + i$ and $N = 102$ sites. Two horseshoe-shaped lines in (d) show regularized PBCs for $N = 101$ and $N = 351$ atoms. Inset illustrates the complex K contour used for regularized PBC. Calculation has been performed for $\xi = 1/2$ and $\varphi = \pi/2$.

an array of N periodically spaced emitters described by the effective non-Hermitian Hamiltonian [18] $H = \sum_{m,n=1}^N H_{m,n} \sigma_n^\dagger \sigma_m$ with σ_m^\dagger being the raising operators and

$$H_{m,n} = \omega_0 \delta_{m,n} - i \begin{cases} \gamma_{\rightarrow} e^{i\varphi|m-n|}, & m > n \\ \frac{\gamma_{\rightarrow} + \gamma_{\leftarrow}}{2}, & m = n \\ \gamma_{\leftarrow} e^{i\varphi|m-n|}, & m < n \end{cases} \quad (1)$$

where $\gamma_{\rightarrow} = 2\gamma_{1D}/(1 + \xi)$, $\gamma_{\leftarrow} = 2\gamma_{1D}\xi/(1 + \xi)$, are the spontaneous emission rates into the waveguide in the forward and backward directions. The phase $\varphi = \omega_0 d/c$ is the phase gained by light between the two emitters. We use the Markovian approximation, valid for $\gamma_{1D} \ll \omega$, so that the frequency dependence of φ is ignored. Notably, the Hamiltonian Eq. (1) features long-range photon-mediated coupling between distant emitters. The parameter ξ is the ratio of emission rates in the forward and backward directions. Under the PBC, the Hamiltonian matrix H_{mn} has the eigenstates $\psi_m = e^{iK_m}$ with the eigenenergies

$$\omega(K) = \omega_0 + \gamma_{1D} \frac{\sin \varphi + c \sin K}{\cos K - \cos \varphi}, \quad \text{where } c = \frac{1 - \xi}{1 + \xi}. \quad (2)$$

Importantly, the energy spectrum Eq. (2) is purely real. It features a singularity near the light line, $K = \varphi$, and a polaritonic band gap near the emitter resonance frequency ω_0 . We can also rewrite the dispersion law in the effective medium approximation, assuming $\varphi \ll 1$, $K \ll 1$, that leads to $K^2 = \varphi^2 \varepsilon(\omega, K)$ where

$$\varepsilon(\omega, K) = 1 + \frac{2\gamma_{1D}}{\varphi} \frac{1 + cK}{\omega_0 - \omega} \quad (3)$$

is the resonant permittivity. The breakdown of the time-reversal symmetry for $c \neq 0$ is manifested by the linear-in- K term in Eq. (3).

The OBC spectrum can be obtained either directly by diagonalizing Eq. (1) or by solving the equation [19, 24]

$$r_{\rightarrow}(\omega) r_{\leftarrow}(\omega) e^{i(K_+ - K_-)(N-1)} = 1 \quad (4)$$

where $r_{\rightarrow/\leftarrow} = -(e^{\pm iK_{\pm}} - e^{i\varphi})/(e^{\pm iK_{\mp}} - e^{i\varphi})$ are the reflection coefficients of the polaritonic modes from the inside of the structure and K_{\pm} are the solutions for the dispersion equation for forward and backward propagating waves. Equation (4) describes standing waves in the cavity made of resonant chiral material with the (effective) permittivity Eq. (3). The chiral WQED is related to the non-reciprocal waveguide system [25], that has attracted a lot of interest [26–29].

Mesoscopic NHSE. Figure 2 presents the eigenstates and the OBC spectra calculated for the finite arrays with $N = 101$ emitters for two different asymmetry parameters $\xi = 0.5$ (a,b) and $\xi = 0.05$ (c,d). In both cases, the structures feature superradiant modes with a much larger decay rate than the single atom decay rate γ_{1D} [19].

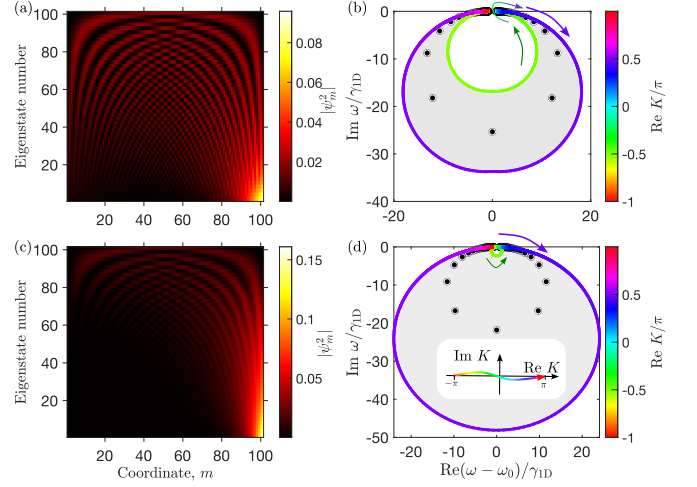


FIG. 2. Eigenmodes (a,c) and energy spectrum (c,d) of the structure with $N = 101$ emitters and $\xi = 0.5$ (a,b) and $\xi = 0.05$ (c,d). Filled circles correspond to the numerical solution, open circles are calculated according to Eq. (6). The eigenmodes in (a,b) are presented in the descending order of the radiative decay rate. The PBC spectrum is shown by colored lines in (c,d). Inset in (d) schematically illustrates the complex K contour used for the PBC calculation.

The eigenmodes in Fig. 2(a,c) are ordered by the decreasing radiative decay rate and it is clear that they become pinned to the edges for higher decay rate. In the more chiral case, Fig. 2(c), the large fraction of eigenmodes is concentrated at just one edge, which looks like the hallmark of the NHSE. Indeed, increasing the imaginary part of ω suppresses the resonant reflection coefficients $r_{\rightarrow/\leftarrow}$ which means easier photon escape outside of the structure. At the same time, the difference between $\text{Im } K_+$ and $\text{Im } K_-$ increases in the presence of the chirality. Given the eigenmode spatial profile [19]

$$\psi_m \propto e^{iK_+(m-N)} + r_{\leftarrow} e^{iK_-(m-N)} \propto e^{iK_+(m-1)} r_{\rightarrow} + e^{iK_-(m-1)}, \quad (5)$$

the increase of this difference means localization of the eigenmodes at one particular edge. For $|\omega - \omega_0| \gg \gamma_{1D}$ and $\varphi = \pi/2$ we can obtain from Eq. (4) an approximate analytical expression for the OBC spectrum

$$\omega_{\nu}^{\pm} - \omega_0 = -\frac{iN\gamma_{1D}}{W_{\nu}(\pm 2N/\sqrt{1 - c^2})}, \quad \nu = 0, \pm 1, \pm 2 \dots \quad (6)$$

of the most superradiant modes, which is shown by open circles in Fig. 2(b,d) and well describes the numerical results. Here, $W_{\nu}(z)$ is the Lambert function, satisfying the equation $W_{\nu} e^{W_{\nu}} = z$. For $N \gg 1$ we can approximate it as $W(z) \approx \ln z - \ln \ln z - i\pi\nu z$, which makes evident a weak logarithmic suppression of the linear growth of the radiative decay rate with N . Such suppression is distinct from the usual single superradiant Dicke mode for $\varphi = 0$, see also Ref. [30] for more detail on the $\varphi = 0$ case.

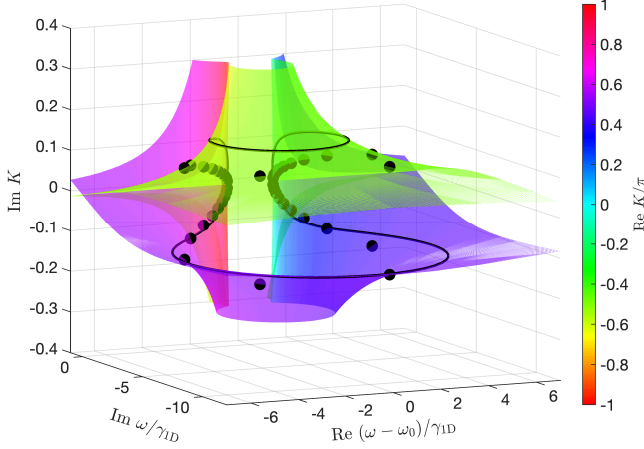


FIG. 3. Riemann surface of the dispersion law $\omega(K)$. Color indicates the value of $\text{Re } K$. Dots show the values of K_{\pm} for the eigenfrequencies of the finite structure ω . Thick black line corresponds to the contour $K = \text{Re } K - i0.13\pi \sin \text{Re } K$. Calculation has been performed for $\xi = 0.5$ ($c = 1/3$), $\varphi = \pi/2$ and $N = 20$.

The presence of edge-concentrated eigenmodes in the finite structures has inspired us for more detailed analysis of the PBC energy spectra. The $N \rightarrow \infty$ limit of infinite structure with purely zero loss is not well defined. Even in vacuum, the photon propagator $1/[(\omega/c)^2 - K^2]$ has a singularity in K space that has to be carefully treated if one needs for example, to use the Cauchy theorem to integrate over K or ω [31]. Here we consider the excitations with $\text{Im } \omega < 0$ that decay in time $\propto \exp(-i\omega t)$, and one should add the imaginary part to the wave vector K with an appropriate sign. We propose the regularization

$$K \rightarrow \text{Re } K - i\delta K(N) \sin \text{Re } K, -\pi \leq \text{Re } K < \pi \quad (7)$$

for the dispersion law Eq. (2). The small parameter $\delta K(N)$ accounts for the finite (radiative) losses that render the PBC spectrum Eq. (2) complex. The horseshoe-like contour of the regularized PBC is shown in Fig. 1(a) and Fig. 2(b,d) by lines with gradient color that encodes the value of $\text{Re } K$. This regularized PBC spectrum has a loop around the OBC characterized by the nonvanishing winding number. For vanishing chirality, when $\omega(K) = \omega(-K)$, the horseshoe shrinks to a line with zero area and for larger chirality it expands to a full circle (Fig. 2d). Contrary to the usual NHSE case, the regularization parameter δK in Eq. (7) is not universal. It depends on N and tends to zero for $N \rightarrow \infty$. The curves in Fig. 1(d) and Fig. 2 have been calculated for $\delta K = 4/N$. This scaling describes how for larger N the horseshoe expands and at the same time the ends of the horseshoe approach the real-valued PBC spectrum, see Fig. 1(d). Numerical analysis hints at a more complicated scaling $\delta K \propto \ln N/N$, which reflects the dependence of the lifetime of the modes Eq. (6) on N .

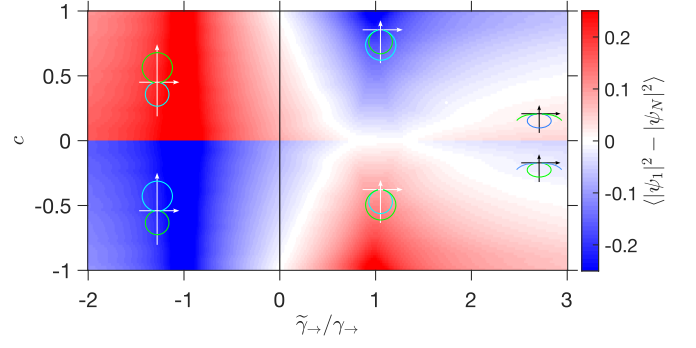


FIG. 4. Localization of the eigenmodes at the edges depending on the loss parameter $\tilde{\gamma}_{\rightarrow}$ and the chirality degree c . The insets schematically illustrate the regularized PBC spectra. The calculation has been performed for $\varphi = \pi/2$ and $N = 20$.

It is also instructive to analyze the Riemann surface of $\omega(K)$ that is shown in Fig. 3 depending on both $\text{Re } K$ and $\text{Im } K$ together with the OBC energy spectrum and the regularization path Eq. (7). The color of the Riemann surface encodes the value of $\text{Re } K$. In such a way, it becomes evident that the non-zero winding is the generic feature of the complex energy spectrum of the chiral structure that is independent of the particular regularization. On the other hand, Fig. 3 also demonstrates a clear distinction from the usual systems with NHSE: the signs of $\text{Im } K_{+}$ and $\text{Im } K_{-}$ for the OBC eigenmodes are opposite. The eigenmode localization at one particular edge, apparent in Fig. 2(c), is just due to the different weight of the terms $\propto e^{iK_{\pm}m}$ in Eq. (5) and not because both exponents decay into the same direction.

The control of the mesoscopic NHSE by the losses or gain through the edges can be explicitly demonstrated by analyzing the non-Hermitian part of the Hamiltonian Eq. (1)

$$H_{nm} - H_{mn}^{*} = -i\gamma_{\rightarrow} e^{i\varphi(n-m)} - i\gamma_{\leftarrow} e^{i\varphi(m-n)}.$$

The presence of just two terms in the singular value decomposition of $H - H^{\dagger}$ is yet another manifestation of the unusual nature of considered non-Hermiticity; they describe emission to the right and to the left [32]. It is instructive to explicitly modify the γ_{\rightarrow} coefficient in the non-Hermitian part, $\gamma_{\rightarrow} \rightarrow \tilde{\gamma}_{\rightarrow}$. We assume this can be realized by controlling the medium outside the structure. The results are presented in Fig. 4, where the color encodes the edge localization degree $|\psi_1|^2 - |\psi_N|^2$, averaged over all the eigenstates ψ . For completeness, we also considered the case $\tilde{\gamma}_{\rightarrow} < 0$, which means the presence of the gain. Importantly, the usual PBC spectrum does not depend on $\tilde{\gamma}_{\rightarrow}$, while the regularized PBC does (see the insets in Fig. 4). Thus, Fig. 4 demonstrates that despite the usual PBC spectrum staying real, the modification of the boundary conditions can control the sign of the mesoscopic NHSE by switching the mode localization direction in the finite array.

Summary. To summarize, we show how the concept of nontrivial point-gap topology, usually used under the periodic boundary conditions, can be used to analyze a mesoscopic analog of the non-Hermitian skin effect in a finite-size photonic structure with the only loss or gain being at the edges. While our consideration has been limited to the simplest one-dimensional model, it also hints at possible eigenmode concentration at the edges of various resonant structures, provided they are chiral and lossless inside. These could be, for example, chiral all-dielectric metasurfaces with Mie resonances [33, 34].

Acknowledgments. The work of ANP has been supported by research grants from the Center for New Scientists and from the Center for Scientific Excellence at the Weizmann Institute of Science. S. F. acknowledges a Simons Investigator in Physics grant from the Simons Foundation (Grant No. 827065)

* poddubny@weizmann.ac.il

† janetzh@stanford.edu

- [1] Tony E. Lee, “Anomalous edge state in a non-Hermitian lattice,” *Phys. Rev. Lett.* **116**, 133903 (2016).
- [2] V. M. Martinez Alvarez, J. E. Barrios Vargas, and L. E. F. Foa Torres, “Non-Hermitian robust edge states in one dimension: Anomalous localization and eigenspace condensation at exceptional points,” *Phys. Rev. B* **97**, 121401 (2018).
- [3] Flore K. Kunst, Elisabet Edvardsson, Jan Carl Budich, and Emil J. Bergholtz, “Biorthogonal bulk-boundary correspondence in non-Hermitian systems,” *Phys. Rev. Lett.* **121**, 026808 (2018).
- [4] Shunyu Yao and Zhong Wang, “Edge states and topological invariants of non-Hermitian systems,” *Phys. Rev. Lett.* **121**, 086803 (2018).
- [5] Dan S. Borgnia, Alex Jura Kruchkov, and Robert-Jan Slager, “Non-Hermitian boundary modes and topology,” *Phys. Rev. Lett.* **124**, 056802 (2020).
- [6] Nobuyuki Okuma, Kohei Kawabata, Ken Shiozaki, and Masatoshi Sato, “Topological origin of non-Hermitian skin effects,” *Phys. Rev. Lett.* **124**, 086801 (2020).
- [7] Emil J. Bergholtz, Jan Carl Budich, and Flore K. Kunst, “Exceptional topology of non-Hermitian systems,” *Rev. Mod. Phys.* **93**, 015005 (2021).
- [8] Janet Zhong, Kai Wang, Yubin Park, Viktor Asadchy, Charles C. Wojcik, Avik Dutt, and Shanhui Fan, “Non-trivial point-gap topology and non-Hermitian skin effect in photonic crystals,” *Phys. Rev. B* **104**, 125416 (2021).
- [9] Stefano Longhi, “Non-Hermitian skin effect beyond the tight-binding models,” *Phys. Rev. B* **104**, 125109 (2021).
- [10] Kazuki Yokomizo, Taiki Yoda, and Shuichi Murakami, “Non-Hermitian waves in a continuous periodic model and application to photonic crystals,” *Phys. Rev. Research* **4**, 023089 (2022).
- [11] Kai Wang, Avik Dutt, Ki Youl Yang, Casey C. Wojcik, Jelena Vučković, and Shanhui Fan, “Generating arbitrary topological windings of a non-Hermitian band,” *Science* **371**, 1240–1245 (2021).
- [12] Naomichi Hatano and David R. Nelson, “Vortex pinning and non-Hermitian quantum mechanics,” *Phys. Rev. B* **56**, 8651–8673 (1997).
- [13] Peter Lodahl, Sahand Mahmoodian, Søren Stobbe, Arno Rauschenbeutel, Philipp Schneeweiss, Jürgen Volz, Hannes Pichler, and Peter Zoller, “Chiral quantum optics,” *Nature* **541**, 473–480 (2017).
- [14] Alexandra S. Sheremet, Mihail I. Petrov, Ivan V. Iorsh, Alexander V. Poshakinskiy, and Alexander N. Poddubny, “Waveguide quantum electrodynamics: Collective radiance and photon-photon correlations,” *Rev. Mod. Phys.* **95**, 015002 (2023).
- [15] Adarsh S. Prasad, Jakob Hinney, Sahand Mahmoodian, Klemens Hammerer, Samuel Rind, Philipp Schneeweiss, Anders S. Sørensen, Jürgen Volz, and Arno Rauschenbeutel, “Correlating photons using the collective non-linear response of atoms weakly coupled to an optical mode,” *Nature Photonics* **14**, 719 (2020).
- [16] Christian Liedl, Sebastian Pucher, Felix Tebbenjohanns, Philipp Schneeweiss, and Arno Rauschenbeutel, “Collective radiation of a cascaded quantum system: From timed Dicke states to inverted ensembles,” *Phys. Rev. Lett.* **130**, 163602 (2023).
- [17] Lei Du, Lingzhen Guo, Yan Zhang, and Anton Frisk Kockum, “Giant emitters in a structured bath with non-Hermitian skin effect,” (2023), [arXiv:2308.16148](https://arxiv.org/abs/2308.16148) [quant-ph].
- [18] D. F. Kornovan, M. I. Petrov, and I. V. Iorsh, “Transport and collective radiance in a basic quantum chiral optical model,” *Phys. Rev. B* **96**, 115162 (2017).
- [19] Gleb Fedorovich, Danil Kornovan, Alexander Poddubny, and Mihail Petrov, “Chirality-driven delocalization in disordered waveguide-coupled quantum arrays,” *Phys. Rev. A* **106**, 043723 (2022).
- [20] Mengjie Yang, Luojia Wang, Xiaoxiong Wu, Han Xiao, Danying Yu, Luqi Yuan, and Xianfeng Chen, “Concentrated subradiant modes in a one-dimensional atomic array coupled with chiral waveguides,” *Phys. Rev. A* **106**, 043717 (2022).
- [21] Yi-Cheng Wang, Jhih-Shih You, and H. H. Jen, “A non-Hermitian optical atomic mirror,” *Nat Commun* **13**, 4598 (2022).
- [22] Tao Yu and Bowen Zeng, “Giant microwave sensitivity of a magnetic array by long-range chiral interaction driven skin effect,” *Phys. Rev. B* **105**, L180401 (2022).
- [23] Bowen Zeng and Tao Yu, “Radiation-free and non-hermitian topology inertial defect states of on-chip magnons,” *Phys. Rev. Research* **5**, 013003 (2023).
- [24] M. Voronov, E. Ivchenko, M. Eremenchouk, L. Deych, and A. Lisyansky, “Photoluminescence spectroscopy of one-dimensional resonant photonic crystals,” *J. of Luminescence* **125**, 112–117 (2007).
- [25] K. L. Tsakmakidis, L. Shen, S. A. Schulz, X. Zheng, J. Upham, X. Deng, H. Altug, A. F. Vakakis, and R. W. Boyd, “Breaking Lorentz reciprocity to overcome the time-bandwidth limit in physics and engineering,” *Science* **356**, 1260–1264 (2017).
- [26] Sander A. Mann, Dimitrios L. Sounas, and Andrea Alù, “Nonreciprocal cavities and the time-bandwidth limit,” *Optica* **6**, 104–110 (2019).
- [27] Kosmas L. Tsakmakidis, Yun You, Tomasz Stefański, and Linfang Shen, “Nonreciprocal cavities and the time-bandwidth limit: comment,” *Optica* **7**, 1097 (2020).
- [28] Sander A. Mann, Dimitrios L. Sounas, and Andrea Alù, “Nonreciprocal cavities and the time-bandwidth limit:

- reply,” *Optica* **7**, 1102 (2020).
- [29] Siddharth Buddhiraju, Yu Shi, Alex Song, Casey Wojcik, Momchil Minkov, Ian A. D. Williamson, Avik Dutt, and Shanhui Fan, “Absence of unidirectionally propagating surface plasmon-polaritons at nonreciprocal metal-dielectric interfaces,” *Nat Commun* **11**, 674 (2020).
 - [30] Yi-Cheng Wang, H. H. Jen, and Jhih-Shih You, “Scaling laws for non-Hermitian skin effect with long-range couplings,” *Phys. Rev. B* **108**, 085418 (2023).
 - [31] V.B. Berestetskii, E.M. Lifshitz, and L.P. Pitaevskii, *Quantum Electrodynamics: Volume 4*, Vol. 4 (Butterworth-Heinemann, 1982).
 - [32] Silvia Cardenas-Lopez, Stuart J. Masson, Zoe Zager, and Ana Asenjo-Garcia, “Many-body superradiance and dynamical mirror symmetry breaking in waveguide QED,” *Phys. Rev. Lett.* **131**, 033605 (2023).
 - [33] Yuri Kivshar, “Mie scattering yields chiral nonlinearity,” *Nature Photonics* **16**, 89–90 (2022).
 - [34] Kirill Koshelev, Yutao Tang, Zixian Hu, Ivan I. Kravchenko, Guixin Li, and Yuri Kivshar, “Resonant chiral effects in nonlinear dielectric metasurfaces,” *ACS Photonics* **10**, 298–306 (2023).